Computational and Theoretical Chemistry 977 (2011) 86–91

Contents lists available at SciVerse ScienceDirect

Computational and Theoretical Chemistry

journal homepage: www.elsevier.com/locate/comptc

Ab initio molecular dynamics investigations on the S_N2 reactions of OH^- with NH_2F and NH_2Cl

Feng Yu [a,b,*], Lei Song [a], Xiaoguo Zhou [a,*]

[a] Hefei National Laboratory for Physical Sciences at the Microscale, Department of Chemical Physics, University of Science and Technology of China, Hefei, Anhui 230026, China
[b] Department of Mathematics and Physics, Xi'an Technological University, Xi'an, Shaanxi 710032, China

ARTICLE INFO

Article history:
Received 21 May 2011
Received in revised form 12 September 2011
Accepted 12 September 2011
Available online 28 September 2011

Keywords:
Hydroxide anion (OH^-)
Fluoroamine (NH_2F)
Chloramine (NH_2Cl)
Bimolecular nucleophilic substitution (S_N2) reaction
Ab initio molecular dynamics

ABSTRACT

The bimolecular nucleophilic substitution (S_N2) reactions of hydroxide anion (OH^-) with fluoroamine (NH_2F) and chloramine (NH_2Cl) have been investigated with *ab initio* molecular dynamics simulations. For the S_N2 reaction of OH^- with NH_2F, there are two main dynamic reaction pathways after passing the $[HO\cdots NH_2\cdots F]^-$ barrier. The first one is that the $[HO\cdots NH_2\cdots F]^-$ transition state directly dissociates to the products of F^- and NH_2OH without involving any dynamic intermediate complex, and on the contrary, the other one involves the dynamic hydrogen bond $F^-\cdots H-NH-OH$ and/or $F^-\cdots H-O-NH_2$ intermediate complexes. As to the S_N2 reaction of OH^- with NH_2Cl, there is only one dominant dynamic reaction pathway, which leads to the products of Cl^- and NH_2OH directly. According to our calculations, the statistical theories including the Rice–Ramsperger–Kassel–Marcus (RRKM) theory and transition state (TS) theory cannot be utilized to model the reaction kinetics for these two S_N2 reactions.

1. Introduction

Bimolecular nucleophilic substitution (S_N2) reactions have been studied both experimentally and theoretically due to their important roles in physical organic chemistry and gas phase negative ion chemistry [1–7]. Compared with the S_N2 reactions at carbon (C) center, the S_N2 reactions at nitrogen (N) center are less understood [7]. However, the S_N2 reactions at N center are very significant in organic synthesis and carcinogenesis [8–11]. Therefore, the S_N2 reactions at N center should be investigated extensively to enrich the knowledge of the S_N2 reactions. Gareyev et al. [12] studied the reactions between several anionic nucleophiles and chloramine (NH_2Cl) by utilizing the tandem flowing afterglow-selected ion flow tube (FA-SIFT) operated at 300 K. The overall reaction rate coefficients and branching ratios for these reactions were measured quantitatively. Bühl and Schaefer [13,14] optimized the geometries of transition states of the S_N2 reactions at N center with *ab initio* methods, and discussed the rate-equilibrium relationships, proton transfer, and steric effects. Moreover, the similarities and differences between the S_N2 reactions at C and N centers were also compared. Minyaev and Wales [15] theoretically studied the topology of the potential energy surface (PES) for the S_N2 reaction between F^- and fluoroamine (NH_2F). As a result, the corresponding gradient line reaction path for the reaction of F^- with NH_2F was mapped. With the development of the quantum chemical methods, more and more theoretical investigations have been done on the topic of the S_N2 reactions at N center in the gas phase [16–25] and even condensed phase [26,27].

The S_N2 reactions of hydroxide anion (OH^-) with NH_2F and NH_2Cl are two typical S_N2 reactions at N center. According to previous experimental conclusions [12], the reaction of OH^- with NH_2Cl was very efficient, and the branching ratios of anionic products were Cl^- (20%) and $NHCl^-$ (80%), which corresponded to the S_N2 and proton transfer reaction channels, respectively. As far as we know, no experimental results have been reported on the reaction of OH^- with NH_2F. The cut-through PESs, i.e., the potential energy profiles for the S_N2 reactions of OH^- with NH_2F and NH_2Cl were explored at the levels of self-consistent field (SCF) method with double zeta polarized (DZP) and augmented DZP basis sets, respectively [14]. Additionally, the proton transfer channel of the $OH^- + NH_2Cl$ reaction was discussed compared with the S_N2 reaction channel [14].

From the calculated cut-through PESs, the static reaction pathways can be obtained to explain the reaction mechanisms of the observed anionic products. Nevertheless, the dynamic reaction

* Corresponding authors. Address: Hefei National Laboratory for Physical Sciences at the Microscale, Department of Chemical Physics, University of Science and Technology of China, Hefei, Anhui 230026, China (F. Yu). Tel.: +86 551 3600031; fax: +86 551 3602323 (X. Zhou).
E-mail addresses: fengyu03@mail.ustc.edu.cn (F. Yu), xzhou@ustc.edu.cn (X. Zhou).

2210-271X/$ - see front matter © 2011 Elsevier B.V. All rights reserved.
doi:10.1016/j.comptc.2011.09.009

pathways involving the animated motion of the atoms in the reactive system cannot be obtained. Especially for the S_N2 reaction, both the static and dynamic reaction pathways are proved to be equally important to uncover the real reaction mechanisms [2,28–31], e.g., the typical S_N2 reaction of OH^- with CH_3F tended to avoid the potential energy well of $CH_3OH\cdots F^-$ on the exit-channel PES and directly dissociate to the products of F^- and CH_3OH, indicating that the dominant dynamic pathway did not follow the minimum energy path (MEP) [28]. In this paper, we mainly employ *ab initio* molecular dynamics [32–34] method to investigate the dynamic reaction pathways for the S_N2 reactions of OH^- with NH_2F and NH_2Cl. Based on our calculations, the dynamic effects on their reaction processes are uncovered. We also compare these two S_N2 reactions with the S_N2 reaction of OH^- with CH_3F, and furthermore, the similar and different dynamic behaviors are extensively discussed.

2. Computational methods

All the present *ab initio* calculations and molecular dynamics simulations were performed with the Gaussian 03 program package [35]. The reactants, products, static intermediate complexes, and transition states on the PESs for the S_N2 reactions of OH^- with NH_2F and NH_2Cl were optimized at the MP2(full) [36,37]/6-31+G(d) level of theory, and then the harmonic frequencies and zero point energies (ZPEs) were calculated at the same level. Moreover, the single point energies of these optimized molecular structures were corrected at the CCSD(T,full) [38]/6-311++G(3df,2p) level, and the unscaled ZPEs at the MP2(full)/6-31+G(d) level were used. Note that the energies at 0 K were utilized in Section 3.1.

The *ab initio* molecular dynamics simulations were carried out with the Born–Oppenheimer molecular dynamics (BOMD) method [33,34] incorporated in the Gaussian 03 program package. This method has been successfully employed by us to show the dynamic effects in the reactions of O^- with CH_3F [39,40] and C_2H_4 [41].

The dynamic trajectories were propagated on the Born–Oppenheimer PES calculated at the MP2(full)/6-31+G(d) level of theory. The trajectories were integrated by using the Hessian-based predictor–corrector algorithm with Hessian updating for five steps [42,43]. The step size of all the trajectories was set as the default value, 0.25 $amu^{1/2}$ bohr. The trajectory would be stopped when the distance of center of mass between any couple of separated fragments was 15 bohr apart or the total integration steps exceeded the maximal points of 3500. The trajectories were initiated at the S_N2 transition states denoted as $[HO\cdots NH_2\cdots F]^-$ and $[HO\cdots NH_2\cdots Cl]^-$. The initial conditions were determined by the thermal [44] and microcanonical [45–47] samplings. The phase of the transition vector was set to point to the products, and thus, most of the dynamic trajectories were propagating on the exit-channel PES. With respect to the thermal samplings, both the vibrational and rotational sampling temperatures were set to be 300 K, and the ZPEs were also included in the vibrational sampling. For the S_N2 reaction of OH^- with NH_2F, the energies added on the transition vector of the $[HO\cdots NH_2\cdots F]^-$ transition state were specified to be values sampled from the thermal distribution at 300 K, 0.6 kcal/mol, and 15.0 kcal/mol, respectively. A total of 105 trajectories were calculated for these three cases. As to the S_N2 reaction of OH^- with NH_2Cl, the energies added on the transition vector of the $[HO\cdots NH_2\cdots Cl]^-$ transition state were only sampled from the thermal distribution at 300 K, and a total of 64 trajectories were calculated for this case. With respect to the microcanonical samplings, the rotational sampling temperature was set as 300 K, and a total energy of 19.7 kcal/mol and 17.9 kcal/mol above the ZPEs was added to the transition vectors and vibrational modes of the transition states of $[HO\cdots NH_2\cdots F]^-$ and $[HO\cdots NH_2\cdots Cl]^-$, respectively. A total of 70 trajectories were calculated for these two cases.

Generally, the total angular momentums for all the 239 trajectories floated within a range of $10^{-9}\hbar$–$10^{-7}\hbar$, and the total energies drifted within a range from 10^{-3} kcal/mol to 1 kcal/mol. The barrier recrossing among these 239 trajectories was very infrequent, and thus, the corresponding discussion was ignored. Additionally, the Mulliken population analysis [48] was used to determine the charge distributions of the products at the end of the dynamic trajectories.

3. Results and discussion

3.1. Static reaction pathways for the S_N2 reactions of OH^- with NH_2F and NH_2Cl

The potential energy profiles at the CCSD(T,full)/6-311++G(3df,2p)//MP2(full)/6-31+G(d) level of theory for the reactions of OH^- with NH_2F and NH_2Cl are depicted in Fig. 1. Our potential energy profiles are consistent with previous theoretical calculations [14]. It should be noted that the optimizations of the hydrogen bond $HO^-\cdots H-NH-Cl$ intermediate complex at the MP2(full)/6-31+G(d,p) and MP2(full)/6-311++G(3df,2p) levels always lead to the hydrogen bond $HO-H\cdots NH-Cl^-$ intermediate complex finally. The proton transfer occurs in the optimization processes at these two levels of theory. However, the discussion on the proton transfer reaction is beyond the scope of this study. Combined with previous theoretical conclusions [14], the static reaction pathway for

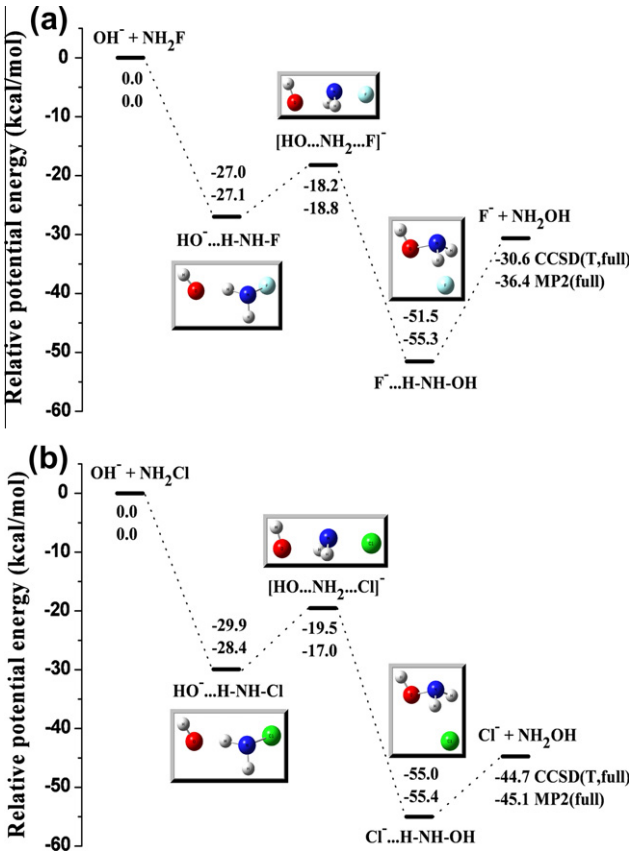

Fig. 1. Potential energy profiles for the S_N2 reactions of OH^- with NH_2F (a) and NH_2Cl (b), where the molecular structures of the critical points on the potential energy profiles are also depicted. The upper values are the calculated energies at the CCSD(T,full)/6-311++G(3df,2p)//MP2(full)/6-31+G(d) level, and the lower data are calculated at MP2(full)/6-31+G(d) level.

the S_N2 reaction of OH^- with NH_2F could be viewed as follows. At first, OH^- attacks one of the H atoms of NH_2F to form the hydrogen bond $HO^-\cdots H-NH-F$ intermediate complex, and then, this intermediate complex overcomes the $[HO\cdots NH_2\cdots F]^-$ barrier to produce another hydrogen bond intermediate complex of $F^-\cdots H-NH-OH$. Subsequently, the $F^-\cdots H-NH-OH$ intermediate will decompose to F^- and NH_2OH as products at last. The static reaction pathway for the S_N2 reaction of OH^- with NH_2Cl is the same as the S_N2 reaction between OH^- and NH_2F.

As shown in Fig. 1, the energies of the various critical points on the potential energy profiles at the MP2(full)/6-31+G(d) level are close to those at the CCSD(T,full)/6-311++G(3df,2p)//MP2(full)/6-31+G(d) level, and thus, using the MP2(full)/6-31+G(d) level to perform *ab initio* molecular dynamics simulations is reasonable.

3.2. Dynamic reaction pathways for the S_N2 reaction of OH^- with NH_2F

A total of 105 trajectories initiated at the $[HO\cdots NH_2\cdots F]^-$ transition state have been calculated for the S_N2 reaction between OH^- and NH_2F with the thermal samplings at 300 K. In order to present the dynamic effect, the energies added on the transition vector of the $[HO\cdots NH_2\cdots F]^-$ transition state are specified as values sampled from the thermal distribution at 300 K, 0.6 kcal/mol, and 15.0 kcal/mol, respectively. 35 trajectories have been calculated for each case. The results of these trajectories are summarized in Table 1. Note that the minor types of trajectories are ignored in the following discussion.

Two dominant types of dynamic reaction pathways after passing the $[HO\cdots NH_2\cdots F]^-$ barrier have revealed by these 105 trajectories. The first one denoted as type I is that the $[HO\cdots NH_2\cdots F]^-$ transition state directly dissociates to F^- and NH_2OH without involving any dynamic intermediate complex. The distances between N atom and F atom along a typical trajectory are shown in Fig. 2. The other type denoted as type II involves dynamic hydrogen bond intermediate complexes. Fig. 3a shows the distances of N atom with F atom and O atom with F atom along a typical trajectory of type II, and nine molecular geometries along this trajectory are also depicted in Fig. 3b. Generally, this type of trajectory points to the final products of F^- and NH_2OH through undergoing dynamic hydrogen bond intermediate complexes of $F^-\cdots H-NH-OH$ and/or $F^-\cdots H-O-NH_2$. Among the trajectories of type II, some stop at one of these two dynamic hydrogen bond intermediate complexes within the maximal integration steps of 3500, however, they will finally dissociate to F^- and NH_2OH with additional integration steps.

As shown in Fig. 1a, a static intermediate complex of $F^-\cdots H-NH-OH$ has been located on the exit-channel PES. The remarkable character of the static $F^-\cdots H-NH-OH$ intermediate complex is the hydrogen bond of $F^-\cdots H-N$, and the dissociation of this hydrogen bond produces F^- and NH_2OH as suggested in the potential energy profile. On the dynamic reaction pathway of type II, the other intermediate complex denoted as $F^-\cdots H-O-NH_2$ is found, which corresponds to another potential well on the exit-channel PES. This intermediate complex has neither been taken into account on the static reaction pathway in Section 3.1 nor in previous theoretical calculations [14]. The prominent character of this dynamic intermediate complex is the hydrogen bond of $F^-\cdots H-O$. It is obvious that the decomposition of the hydrogen bond of $F^-\cdots H-O$ will also lead to the products of F^- and NH_2OH. As illustrated in Fig. 3b, the dynamic intermediate complexes of $F^-\cdots H-NH-OH$ and $F^-\cdots H-O-NH_2$ can generally isomerize to each other via a "roaming" F^- atomic anion on the dynamic reaction pathway of type II. The "roaming" mechanism has been illuminated in the photodissociation dynamics [49–57] and even in some bimolecular reaction processes [39,41,58,59]. In summary, there are two different potential wells on the exit-channel PES for the S_N2 reaction of OH^- with NH_2F, i.e., one is $F^-\cdots H-NH-OH$ and the other is $F^-\cdots H-O-NH_2$. For the dynamic reaction pathways of type II, the dynamic trajectories are generally trapped in these two potential wells for a period of time.

When the energies added on the transition vector of the $[HO\cdots NH_2\cdots F]^-$ transition state are sampled from the thermal distribution at 300 K, 10 trajectories belong to type I and 24 trajectories belong to type II. When the energy added on the transition vector is set to be 0.6 kcal/mol, 10 and 23 trajectories belong to type I and II, respectively. As the energy added on the transition vector is increased to 15.0 kcal/mol, the number of trajectories of type I increases to 18, while the number of trajectories of type II decreases to 16. Therefore, the dynamic reaction pathways are influenced by the energies added on the transition vector of the $[HO\cdots NH_2\cdots F]^-$ transition state, and the potential reason will be discussed in Section 3.5.

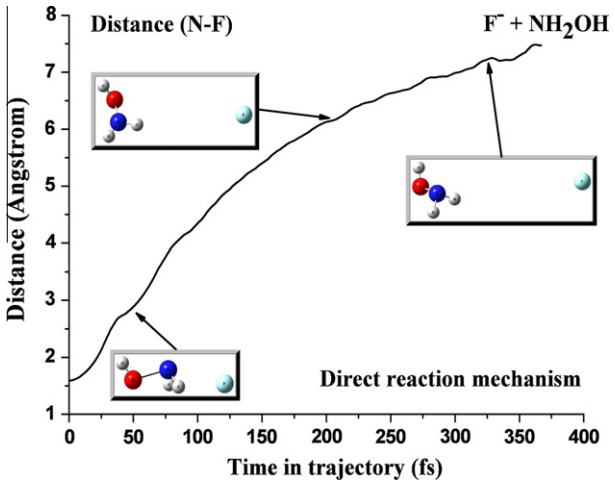

Fig. 2. Distances between N atom and F atom along a typical trajectory of type I on the exit-channel PES for the S_N2 reaction of OH^- with NH_2F. This trajectory directly leads to the products of F^- and NH_2OH without involving any dynamic intermediate complex. Three molecular geometries along this trajectory are also shown.

Table 1
Summary of the dynamic reaction pathways after passing the $[HO\cdots NH_2\cdots F]^-$ barrier for the S_N2 reaction of OH^- with NH_2F with the thermal samplings.

Energies added on the transition vector of the $[HO\cdots NH_2\cdots F]^-$ transition state	$F^- + NH_2OH$ (Type I[a])	$F^- + NH_2OH$ (Type II[b])	Dynamic hydrogen bond intermediate complex (Type II[b])	Other trajectories	Total
Thermal distribution at 300 K	10	9	15	1	35
0.6 kcal/mol	10	9	14	2	35
15.0 kcal/mol	18	8	8	1	35

[a] With respect to this type of trajectory, the $[HO\cdots NH_2\cdots F]^-$ transition state directly dissociates to the final products of F^- and NH_2OH without involving any dynamic intermediate complex.

[b] This type of trajectory leads to the final products of F^- and NH_2OH through undergoing the dynamic hydrogen bond $F^-\cdots H-NH-OH$ and/or $F^-\cdots H-O-NH_2$ intermediate complexes or stops at one of these two dynamic hydrogen bond intermediate complexes within limited maximal integration steps of 3500.

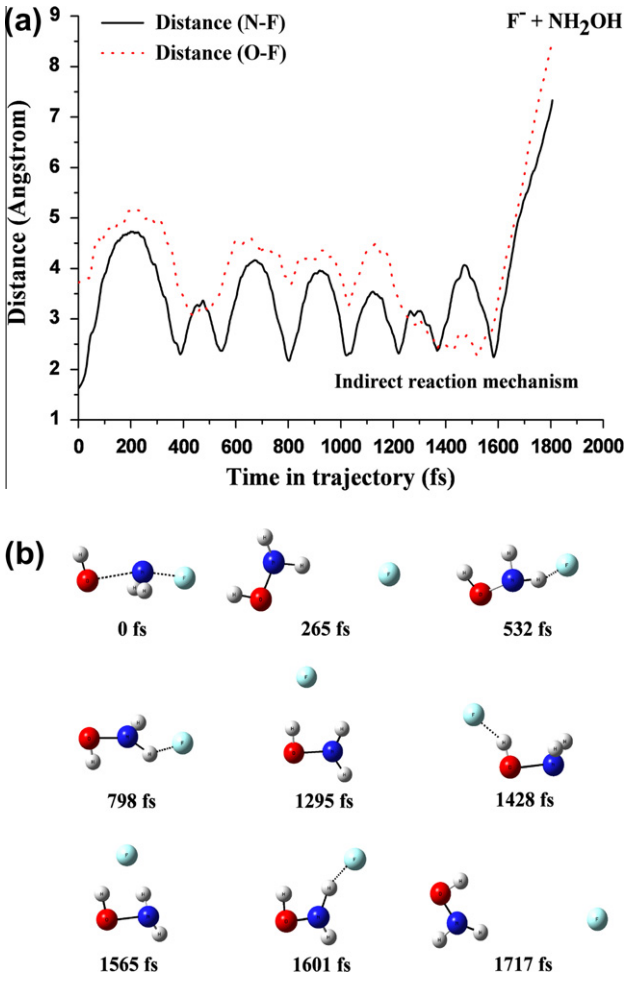

Fig. 3. (a) Distances of N atom with F atom and O atom with F atom along a typical trajectory of type II on the exit-channel PES for the S_N2 reaction of OH^- with NH_2F. This trajectory leads to the products of F^- and NH_2OH through undergoing the dynamic hydrogen bonded $F^-\cdots H-NH-OH$ and $F^-\cdots H-O-NH_2$ intermediate complexes. These two dynamic hydrogen bonded intermediate complexes change to each other via a "roaming" F^- atomic anion. (b) Nine molecular structures along this trajectory.

In order to confirm the dynamic reaction pathways for the S_N2 reaction of OH^- with NH_2F, 35 trajectories have also been calculated with the microcanonical sampling. Among these 35 trajectories, 7 trajectories belong to type I and 20 trajectories belong to type II. The remaining 8 trajectories lead to $H_2O + NHF^-$, $HO-H\cdots NHF^-$ intermediate complex, $NH_2O^- + HF$, and $NH_2O^-\cdots HF$ intermediate complex with small branching ratios. Therefore, the results of the thermal and microcanonical samplings are consistent with each other.

3.3. Dynamic reaction pathways for the S_N2 reaction of OH^- with NH_2Cl

To present the dynamic reaction pathways after passing the $[HO\cdots NH_2\cdots Cl]^-$ barrier for the S_N2 reaction of OH^- with NH_2Cl, a total of 64 trajectories have been calculated with the thermal sampling at 300 K. The energy added on the transition vector of the $[HO\cdots NH_2\cdots Cl]^-$ transition state is sampled from the thermal distribution at 300 K, which corresponds to ~0.6 kcal/mol. Among the 64 trajectories, 57 trajectories (~89%) directly decompose to the products of Cl^- and NH_2OH without involving any dynamic intermediate complex. The distances between N atom and Cl atom along a typical trajectory in these 57 trajectories are shown in Fig. 4. Only 2 trajectories involve the dynamic hydrogen bond $Cl^-\cdots H-NH-OH$ and $Cl^-\cdots H-O-NH_2$ intermediate complexes. Additionally, the other 5 trajectories lead to the $OH^-\cdots H-NH-Cl$ intermediate complex on the entrance-channel PES, and then, the final products of $H_2O + NHCl^-$ are expected through the proton transfer process. It should be noted that the trajectories without involving any dynamic hydrogen bond intermediate complexes would be expected more and more dominant with the energy added on the transition vector increasing.

Additionally, 35 trajectories have been calculated with the microcanonical sampling. Among these 35 trajectories, 27 trajectories (~77%) directly dissociate to the products of Cl^- and NH_2OH without involving any dynamic intermediate complex, and only 1 trajectory involves the dynamic hydrogen bond $Cl^-\cdots H-NH-OH$ and $Cl^-\cdots H-O-NH_2$ intermediate complexes. The rest 7 trajectories firstly lead to the region of $OH^-\cdots H-NH-Cl$ intermediate complex on the entrance-channel PES, and then form the products of $H_2O + NHCl^-$ or the $HO-H\cdots NHCl^-$ intermediate complex through the proton transfer process. The previous theoretical work [14] has discussed the proton transfer channel of the $OH^- + NH_2Cl$ reaction, however, the dynamic effect on this reaction process is beyond the scope of the present study.

3.4. Comparisons with the S_N2 reaction of OH^- with CH_3F

Since the S_N2 reactions at C center and N center are similar, we would like to compare the title reactions with the S_N2 reaction of OH^- with CH_3F [28], and try to understand their dynamic features deeply. As shown by the dynamic trajectory calculations at the MP2/6-31+G(d) level of theory for the $OH^- + CH_3F$ reaction, the most of the trajectories (~90%) avoid the potential energy minimum of $CH_3OH\cdots F^-$ and directly decompose to the products of F^- and CH_3OH [28]. Significantly, this dynamic behavior originates from the "*weak coupling between $CH_3OH + F^-$ relative translation and $O-C\cdots F^-$ bending and other vibrational degrees of freedom of the reactive system*" [28]. The dynamic behavior of the S_N2 reaction of OH^- with NH_2Cl is very similar to the S_N2 reaction of OH^- with CH_3F, which avoids the potential energy minimums of $Cl^-\cdots H-NH-OH$ and $Cl^-\cdots H-O-NH_2$ on the exit-channel PES and directly leads to the products of Cl^- and NH_2OH. Thus, the coupling between $NH_2OH + Cl^-$ relative translation and vibrational degrees

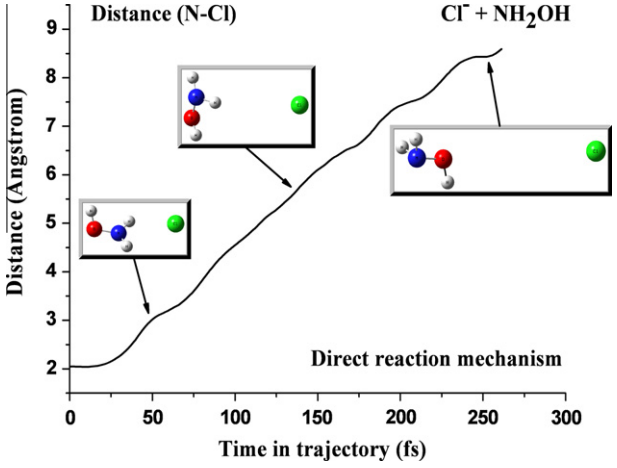

Fig. 4. Distances between N atom and Cl atom along a typical trajectory on the exit-channel PES for the S_N2 reaction of OH^- with NH_2Cl. Along this trajectory, the $[HO\cdots NH_2\cdots Cl]^-$ transition state directly decomposes to the products of Cl^- and NH_2OH without involving any dynamic intermediate complex. Molecular structures of three points on this trajectory are also depicted.

of freedom of this reactive system seems as weak as the S_N2 reaction of OH^- with CH_3F. On the contrary, the dynamic behavior of the S_N2 reaction of OH^- with NH_2F is much different from that of the S_N2 reaction of OH^- with CH_3F. The dynamic intermediate complexes of $F^-\cdots H-NH-OH$ and/or $F^-\cdots H-O-NH_2$ play significant roles in the dynamic reaction pathway of type II, indicating that the coupling between $NH_2OH + F^-$ relative translation and vibrational degrees of freedom is stronger than that in the S_N2 reactive systems of $OH^- + CH_3F$ and $OH^- + NH_2Cl$. Moreover, the energies added on the transition vector of the $[HO\cdots NH_2\cdots F]^-$ transition state seriously influence the dynamic behavior. In other words, the branching ratios of the dynamic reaction pathways of type I and II after passing the $[HO\cdots NH_2\cdots F]^-$ barrier could be controlled by the excitation of the corresponding transition vector.

3.5. Driving energies for the dynamic reaction pathways on the exit-channel PES

After passing the S_N2 barrier, the energy added on the transition vector and the release of the potential energy on the reaction coordinate tend to drive the dissociating fragments departing from each other. On the contrary, the ion–dipole interaction energy between these two dissociating fragments prevents them from separating on the exit-channel PES.

For the S_N2 reaction of OH^- with NH_2F, the competition of the aforementioned energies results in the major dynamic reaction pathways of type I and II. As the energy added on the transition vector is increased from 0.6 kcal/mol to 15.0 kcal/mol, the branching ratio of trajectories of type I increases, indicating that the energy added on the transition vector is beneficial to make the reactive system overcome the ion–dipole interaction energy between F^- and NH_2OH on the exit-channel PES. For the S_N2 reaction of OH^- with NH_2Cl, combined with the release of the potential energy on the reaction coordinate, the energy added on the transition vector of the $[HO\cdots NH_2\cdots Cl]^-$ transition state is able to overcome the ion–dipole interaction energy between Cl^- and NH_2OH overwhelmingly, even at the lower value sampled from the thermal distribution at 300 K. Therefore, the most of the trajectories directly lead to the products of Cl^- and NH_2OH without involving any dynamic intermediate. From the viewpoint of the dynamic reaction pathways, the interaction energy of F^- with NH_2OH is much stronger than that of Cl^- with NH_2OH. As shown in Fig. 1, at the CCSD(T,full)/6-311++G(3df,2p)//MP2(full)/6-31+G(d) level, the interaction energy of the $F^-\cdots H-NH-OH$ complex (20.9 kcal/mol) is stronger than that of the $Cl^-\cdots H-NH-OH$ complex (10.3 kcal/mol). Moreover, at the same level, the interaction energy of the $F^-\cdots H-O-NH_2$ complex (28.4 kcal/mol) is stronger than that of the $Cl^-\cdots H-O-NH_2$ complex (12.6 kcal/mol). These calculated interaction energies are consistent with the results revealed by the dynamic reaction pathways.

3.6. Timescales of the reaction processes on the exit-channel PES and nonstatistical mechanism

For the S_N2 reaction of OH^- with NH_2F, after passing the $[HO\cdots NH_2\cdots F]^-$ barrier, there are two different mechanisms to produce the products of F^- and NH_2OH. One is the direct dissociation to F^- and NH_2OH within about 189 fs–681 fs. This type of reaction process is very fast, and hence the intramolecular vibrational redistribution (IVR) is not efficient. Therefore, utilizing the Rice–Ramsperger–Kassel–Marcus (RRKM) theory [60] and/or transition state (TS) theory [60] to model the S_N2 reaction kinetics of OH^- with NH_2F is not appropriate.

The other is the indirect decomposition within about 593 fs–2489 fs, in which the dynamic hydrogen bond intermediate complexes of $F^-\cdots H-NH-OH$ and/or $F^-\cdots H-O-NH_2$ are involved. For a few trajectories of type II, the lifetimes of the dynamic intermediate complexes are very short, and the corresponding reaction timescale is similar to that of the direct dissociation process. During the short lifetime, the dissociating F^- rebounds once or twice, and then, the intermediate complex decomposes to F^- and NH_2OH immediately. For the most trajectories of type II, the lifetimes of the dynamic intermediate complexes are generally around the timescale of picosecond. As shown in Table 1, some trajectories stop at one of the dynamic hydrogen bond intermediate complexes within the limited maximal steps, and thus, these trajectories need longer time to produce the final products of F^- and NH_2OH. Therefore, the statistical models could be only applied for calculating the reaction kinetics in this case.

The $[HO\cdots NH_2\cdots Cl]^-$ transition state directly dissociates to the products of Cl^- and NH_2OH within about 189 fs–553 fs, which is similar to the timescale of the direct S_N2 reaction mechanism of OH^- with NH_2F. The IVR of this reaction process is not efficient, and therefore, both the RRKM and TS theories based on the potential energy profile are not suitable to model the S_N2 reaction kinetics for this reactive system definitely.

4. Conclusions

The gas phase S_N2 reactions of OH^- with NH_2F and NH_2Cl have been investigated with *ab initio* molecular dynamics simulations. The dynamic reaction pathways and corresponding reaction mechanisms are obtained. For the S_N2 reaction of OH^- with NH_2F, there are two different reaction mechanisms after passing the $[HO\cdots NH_2\cdots F]^-$ barrier. The first one is the direct reaction mechanism, i.e., the $[HO\cdots NH_2\cdots F]^-$ transition state directly dissociates to the products of F^- and NH_2OH without involving any dynamic intermediate complex. On the contrary, the other one is the indirect reaction mechanism, which involves the dynamic hydrogen bonded $F^-\cdots H-NH-OH$ and/or $F^-\cdots H-O-NH_2$ intermediate complexes. For the S_N2 reaction of OH^- with NH_2Cl, there is only one dominant dynamic reaction pathway, which leads to the products of Cl^- and NH_2OH directly. As illuminated by our simulations, the competition between the energy added on the transition vector combined with the release of the potential energy on the reaction coordinate and the interaction energy between the dissociating fragments on the exit-channel PES is the key factor for the dynamic reaction mechanisms. Moreover, in view of the direct reaction mechanism, employing the RRKM theory and/or TS theory to model the S_N2 reaction kinetics of OH^- with NH_2F and NH_2Cl is not appropriate.

Acknowledgment

The financial supports from the National Natural Science Foundation of China (NSFC, Nos. 20603033, 10979042) and National Key Basic Research Special Foundation (NKBRSF, No. 2007CB815204) are gratefully acknowledged. Additionally, F. Yu thanks the Xi'an Technological University for the financial support (No. XAGDXJJ1030), and X. Zhou specially thanks the Fundamental Research Funds for the Central Universities (No. WK2060030006).

References

[1] S.S. Shaik, H.B. Schlegel, S. Wolfe, Theoretical Aspects of Physical Organic Chemistry: The S_N2 Mechanism, Wiley, New York, 1992.
[2] W.L. Hase, Simulations of gas-phase chemical reactions: applications to S_N2 nucleophilic substitution, Science 266 (1994) 998–1002.
[3] M.L. Chabinyc, S.L. Craig, C.K. Regan, J.I. Brauman, Gas-phase ionic reactions: dynamics and mechanism of nucleophilic displacements, Science 279 (1998) 1882–1886.
[4] J.K. Laerdahl, E. Uggerud, Gas phase nucleophilic substitution, Int. J. Mass Spectrom. 214 (2002) 277–314.

[5] S. Schmatz, Quantum dynamics of gas-phase S_N2 reactions, ChemPhysChem 5 (2004) 600–617.
[6] Y. Ren, S.Y. Chu, Recent development in the study of S_N2 reactions at heteroatoms and ion pair systems, J. Theor. Comput. Chem. 5 (2006) 121–140.
[7] S.M. Bachrach, Computational Organic Chemistry, Wiley, New Jersey, 2007.
[8] E. Erdik, M. Ay, Electrophilic amination of carbanions, Chem. Rev. 89 (1989) 1947–1980.
[9] R. Ulbrich, M. Famulok, F. Bosold, G. Boche, S_N2 at nitrogen: the reaction of N-(4-cyanophenyl)-O-diphenylphosphinoylhydroxylamine with N-Methylaniline. A model for the reactions of ultimate carcinogens of aromatic amines with (bio) nucleophiles, Tetrahedron Lett. 31 (1990) 1689–1692.
[10] J.S. Helmick, K.A. Martin, J.L. Heinrich, M. Novak, Mechanism of the reaction of carbon and nitrogen nucleophiles with the model carcinogens O-pivaloyl-N-arylhydroxylamines: competing S_N2 substitution and S_N1 solvolysis, J. Am. Chem. Soc. 113 (1991) 3459–3466.
[11] T. Sheradsky, L. Yusupova, Intramolecular nucleophilic substitution on nitrogen. A new heterocyclic synthesis, Tetrahedron Lett. 36 (1995) 7701–7704.
[12] R. Gareyev, S. Kato, V.M. Bierbaum, Gas phase reactions of NH_2Cl with anionic nucleophiles: nucleophilic substitution at neutral nitrogen, J. Am. Soc. Mass Spectrom. 12 (2001) 139–143.
[13] M. Bühl, H.F. Schaefer III, Theoretical characterization of the transition structure for an S_N2 reaction at neutral nitrogen, J. Am. Chem. Soc. 115 (1993) 364–365.
[14] M. Bühl, H.F. Schaefer III, S_N2 reaction at neutral nitrogen: transition state geometries and intrinsic barriers, J. Am. Chem. Soc. 115 (1993) 9143–9147.
[15] R.M. Minyaev, D.J. Wales, Gradient line reaction path for an S_N2 reaction at neutral nitrogen, J. Phys. Chem. 98 (1994) 7942–7944.
[16] M.N. Glukhovtsev, A. Pross, L. Radom, Gas-phase identity S_N2 reactions of halide ions at neutral nitrogen: a high-level computational study, J. Am. Chem. Soc. 117 (1995) 9012–9018.
[17] Y. Ren, J.L. Wolk, S. Hoz, The performance of density function theory in describing gas-phase S_N2 reactions at saturated nitrogen, Int. J. Mass Spectrom. 221 (2002) 59–65.
[18] Y. Ren, H. Basch, S. Hoz, The periodic table and the intrinsic barrier in S_N2 reactions, J. Org. Chem. 67 (2002) 5891–5895.
[19] Y. Ren, S.Y. Chu, A comprehensive theoretical study on the identity ion pair S_N2 reactions of LiX with NH_2X (X = F, Cl, Br and I), structure, mechanism and potential energy surface, Chem. Phys. Lett. 376 (2003) 524–531.
[20] J. Yang, Y. Ren, H.J. Zhu, S.Y. Chu, Gas-phase non-identity S_N2 reactions at neutral nitrogen: a hybrid DFT study, Int. J. Mass Spectrom. 229 (2003) 199–208.
[21] Y. Ren, S.Y. Chu, Ion pair S_N2 reactions at nitrogen: a high-level G2M(+) computational study, J. Phys. Chem. A 108 (2004) 7079–7086.
[22] Y. Ren, H.J. Zhu, A G2(+) level investigation of the gas-phase non-Identity S_N2 reactions of halides with halodimethylamine, J. Am. Soc. Mass Spectrom. 15 (2004) 673–680.
[23] Y.M. Xing, X.F. Xu, Z.S. Cai, X.Z. Zhao, DFT study on the behavior and reactivity of electron transfer in gas-phase symmetric $X_a^- + NH_2X_b \rightarrow X_aNH_2 + X_b^-$ (X = F, Cl, Br and I) reactions, J. Mol. Struct.: THEOCHEM 671 (2004) 27–37.
[24] Y.M. Xing, X.F. Xu, Z.S. Cai, X.Z. Zhao, J.P. Cheng, Correlation between the energy and electron density representations of reactivity: mPW1K study of the asymmetric S_N2 reactions at the saturated nitrogen, Chem. Phys. 298 (2004) 125–134.
[25] Y. Zeng, Y. Ren, Theoretical study of intramolecular nucleophilic substitution on nitrogen, Chin. J. Chem. Phys. 18 (2005) 918–924.
[26] H. Liu, F. Müller-Plathe, W.F. van Gunsteren, Molecular dynamics with a quantum-chemical potential: solvent effects on an S_N2 reaction at nitrogen, Chem. Eur. J. 2 (1996) 191–195.
[27] D.P. Geerke, S. Thiel, W. Thiel, W.F. van Gunsteren, Combined QM/MM molecular dynamics study on a condensed-phase S_N2 reaction at nitrogen: the effect of explicitly including solvent polarization, J. Chem. Theory Comput. 3 (2007) 1499–1509.
[28] L. Sun, K. Song, W.L. Hase, A S_N2 reaction that avoids its deep potential energy minimum, Science 296 (2002) 875–878.
[29] U. Lourderaj, K. Park, W.L. Hase, Classical trajectory simulations of post-transition state dynamics, Int. Rev. Phys. Chem. 27 (2008) 361–403.
[30] U. Lourderaj, W.L. Hase, Theoretical and computational studies of non-RRKM unimolecular dynamics, J. Phys. Chem. A 113 (2009) 2236–2253.
[31] H. Yamataka, Molecular dynamics simulations and mechanism of organic reactions: non-TST behaviors, Adv. Phys. Org. Chem. 44 (2010) 173–222.
[32] K. Bolton, W.L. Hase, G.H. Peslherbe, Direct dynamics of reactive systems, in: D.L. Thompson (Ed.), Modern Methods for Multidimensional Dynamics Computations in Chemistry, World Scientific, Singapore, 1998, pp. 143–189.
[33] H.B. Schlegel, Exploring potential energy surfaces for chemical reactions: an overview of some practical methods, J. Comput. Chem. 24 (2003) 1514–1527.
[34] H.B. Schlegel, Ab initio molecular dynamics with Born–Oppenheimer and extended Lagrangian methods using atom centered basis functions, Bull. Korean Chem. Soc. 24 (2003) 837–842.
[35] M. J. Frisch et al., Gaussian 03, Revision D.01, Gaussian, Inc., Wallingford CT, 2004.
[36] C. Møller, M.S. Plesset, Note on an approximation treatment for many-electron systems, Phys. Rev. 46 (1934) 618–622.
[37] M.J. Frisch, M. Head-Gordon, J.A. Pople, Semi-direct algorithms for the MP2 energy and gradient, Chem. Phys. Lett. 166 (1990) 281–289.
[38] K. Raghavachari, G.W. Trucks, J.A. Pople, M. Head-Gordon, A fifth-order perturbation comparison of electron correlation theories, Chem. Phys. Lett. 157 (1989) 479–483.
[39] F. Yu, L.X. Wu, S.L. Liu, X.G. Zhou, Static and dynamic reaction pathways involved in the reaction of O^- and CH_3F, J. Mol. Struct.: THEOCHEM 947 (2010) 1–8.
[40] L.X. Wu, F. Yu, J. Liu, J.H. Dai, X.G. Zhou, S.L. Liu, Ab initio molecular dynamics investigation on the production channels for the reaction of O^- with CH_3F, Acta Phys. Chim. Sin. 26 (2010) 2331–2336.
[41] F. Yu, L.X. Wu, L. Song, X.G. Zhou, S.L. Liu, Dynamic reaction pathways of anionic products on the exit-channel potential energy surface for the reaction of O^- with C_2H_4, J. Mol. Struct.: THEOCHEM 958 (2010) 41–47.
[42] J.M. Millam, V. Bakken, W. Chen, W.L. Hase, H.B. Schlegel, Ab initio classical trajectories on the Born–Oppenheimer surface: Hessian-based integrators using fifth-order polynomial and rational function fits, J. Chem. Phys. 111 (1999) 3800–3805.
[43] V. Bakken, J.M. Millam, H.B. Schlegel, Ab initio classical trajectories on the Born-Oppenheimer surface: updating methods for Hessian-based integrators, J. Chem. Phys. 111 (1999) 8773–8777.
[44] Y.J. Cho, S.R. Vande Linde, L. Zhu, W.L. Hase, Trajectory studies of S_N2 nucleophilic substitution. II. Nonstatistical central barrier recrossing in the $Cl^- + CH_3Cl$ system, J. Chem. Phys. 96 (1992) 8275–8287.
[45] C. Doubleday Jr., K. Bolton, G.H. Peslherbe, W.L. Hase, Direct dynamics simulation of the lifetime of trimethylene, J. Am. Chem. Soc. 118 (1996) 9922–9931.
[46] L. Sun, W.L. Hase, Ab initio direct dynamics trajectory simulation of $C_2H_5F \rightarrow C_2H_4 + HF$ product energy partitioning, J. Chem. Phys. 121 (2004) 8831–8845.
[47] G.H. Peslherbe, H. Wang, W.L. Hase, Monte Carlo sampling for classical trajectory simulations, Adv. Chem. Phys. 105 (1999) 171–201.
[48] R.S. Mulliken, Electronic population analysis on LCAO-MO molecular wavefuctions. I, J. Chem. Phys. 23 (1955) 1833–1840.
[49] D. Townsend, S.A. Lahankar, S.K. Lee, S.D. Chambreau, A.G. Suits, X. Zhang, J. Rheinecker, L.B. Harding, J.M. Bowman, The roaming atom: straying from the reaction path in formaldehyde decomposition, Science 306 (2004) 1158–1161.
[50] P.L. Houston, S.H. Kable, Photodissociation of acetaldehyde as a second example of the roaming mechanism, Proc. Natl. Acad. Sci. U.S.A. 103 (2006) 16079–16082.
[51] A.G. Suits, S.D. Chambreau, S.A. Lahankar, State-correlated DC slice imaging of formaldehyde photodissociation: roaming atoms and multichannel branching, Int. Rev. Phys. Chem. 26 (2007) 585–607.
[52] A.G. Suits, Roaming atoms and radicals: a new mechanism in molecular dissociation, Acc. Chem. Res. 41 (2008) 873–881.
[53] L.B. Harding, Y. Georgievskii, S.J. Klippenstein, Roaming radical kinetics in the decomposition of acetaldehyde, J. Phys. Chem. A 114 (2010) 765–777.
[54] J.M. Bowman, B.C. Shepler, Roaming radicals, Annu. Rev. Phys. Chem. 62 (2011) 531–553.
[55] N. Herath, A.G. Suits, Roaming radical reactions, J. Phys. Chem. Lett. 2 (2011) 642–647.
[56] B.C. Shepler, Y. Han, J.M. Bowman, Are roaming and conventional saddle points for H_2CO and CH_3CHO dissociation to molecular products isolated from each other?, J Phys. Chem. Lett. 2 (2011) 834–838.
[57] H. Xiao, S. Maeda, K. Morokuma, Excited-state roaming dynamics in photolysis of a nitrate radical, J. Phys. Chem. Lett. 2 (2011) 934–938.
[58] J. Mikosch, S. Trippel, C. Eichhorn, R. Otto, U. Lourderaj, J.X. Zhang, W.L. Hase, M. Weidemüller, R. Wester, Imaging nucleophilic substitution dynamics, Science 319 (2008) 183–186.
[59] T. Takayanagi, T. Tanaka, Roaming dynamics in the $MgH + H \rightarrow Mg + H_2$ reaction: quantum dynamics calculations, Chem. Phys. Lett. 504 (2011) 130–135.
[60] T. Baer, W.L. Hase, Unimolecular Reaction Dynamics Experiments and Theory, Oxford University Press, New York, 1996. pp. 171–281.